Potentiometric Gas Sensors for Oxidic Gases

NOBORU YAMAZOE & NORIO MIURA

Department of Molecular and Material Sciences, Graduate School of Engineering Sciences, Kyushu University Kasuga-shi, Fukuoka 816-8580 Japan

Abstract. Solid electrolyte-based electrochemical devices combined with an auxiliary phase of oxyacid salt have, in this decade, emerged as new attractive sensors to detect oxidic gases of CO_2, NO, NO_2 and SO_2. Various combinations of solid electrolytes and auxiliary phases as well as various new single or multi-component auxiliary phases have been exploited to improve the gas sensing properties and stability of these devices. Some of the potentiometric sensors developed e.g., CO_2 sensors using NASICON and Li_2CO_3-$CaCO_3$, NO_2 sensors using NASICON and $NaNO_2$-Li_2CO_3 and SO_2 sensors using MgO-stabilized zirconia and Li_2SO_4-$CaSO_4$-SiO_2, exhibit excellent gas sensing performances in laboratory tests and appear to be promising for monitoring the respective gases in ambient environments and/or combustion exhausts. This paper aims at describing our exploratory works on and the state of the art of these potentiometric gas-sensing devices.

Keywords: gas sensor, CO_2, NO_x, SO_2, solid elecrolyte

1. Introduction

Sensory detection of oxidic gases such as CO_2, NO and NO_2 (NO_x), and SO_2 has become increasing important for protecting global as well as living environments. For the past 10 years, we have been seeking solid-state sensors capable of detecting these oxidic gases in combustion exhausts and environments. It has turned out that electrochemical gas sensors using solid electrolytes exhibit very attractive features, showing promise for applications. It is the aim of this article to review some of our approaches in this field briefly and to describe the state of the art of electrochemical oxidic gas sensors. Let us begin with a description of progress in the conception of electrochemical gas sensors.

2. Types of Potentiometric Gas Sensors

An all-solid-state electrochemical cell is usually constructed by combining a membrane of solid electrolyte (ionic conductor) with a pair of electrodes (electronic conductor). For the past three decades, various electrochemical gas sensors have been developed or proposed. Those sensors are classified into potentiometric and amperometric sensors, and the former group is further divided into equilibrium- and mixed-potential types. We consider here the equilibrium potential type only. The gas sensors of this type have been explored extensively by using conventional as well as unconventional solid electrolytes.

2.1 Type I Sensors

A gas sensor is readily constructed from a solid electrolyte for which the mobile ion is the same as that electrochemically derived from the gas phase. Sensors of this type belong to Type I according to the classification by Weppner [1]. A representative example would be an oxygen sensor using an O^{2-} ionic conductor such as yttria-stabilized zirconia (YSZ). The sensor forms an oxygen concentration cell as follows.

$$O_2, Pt \ ^I| \ YSZ \ |^{II} \ Pt, O_2 \qquad (1)$$
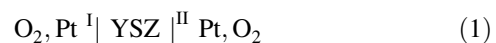
At the three-phase contact between solid electrolyte, electrode (Pt) and gas phase, the following electrochemical reaction proceeds.

$$O_2 + 4e = 2O^{2-} \tag{2}$$

When the partial pressure of oxygen is $P_{O_2}^I$ and $P_{O_2}^{II}$ at the interfaces I and II, respectively, the electromotive force (EMF) of the cell is given by the Nernst equation.

$$E = \frac{RT}{4F} \ln \frac{P_{O_2}^{II}}{P_{O_2}^I} \tag{3}$$

Here F is the Faraday constant, R the gas constant and T the temperature. If $P_{O_2}^I$ is known, one can evaluate $P_{O_2}^{II}$ from the value of E. Type I sensors are also available for simple gases such as H_2, Cl_2, and Na (vapor) by using appropriate conductors of H^+, Cl^- and Na^+. For the oxidic gases like CO_2, however, there are no such solid electrolytes available.

2.2   Type II Sensors

An important breakthrough came about in oxidic gas sensors when Gauthier and Chamberland reported detection of CO_2, NO_2 and SO_2 with electrochemical cells using salts of oxyacids like K_2CO_3, $Ba(NO_3)_2$ and Na_2SO_4 [2,3]. The cell for CO_2, for example, was fabricated on a disc (membrane) of K_2CO_3 as follows.

$$CO_2 - O_2, Au \ ^I | \ K_2CO_3 \ |^{II} \ Au, CO_2 - O_2 \tag{4}$$
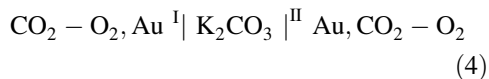
Here K_2CO_3 acts as a solid electrolyte allowing K^+-ionic conduction though at a rather poor conductivity. The gaseous components interact with the electrode (Au) and K_2CO_3 to undergo an electrochemical reaction as follows.

$$2K^+ + CO_2 + \frac{1}{2}O_2 + 2e = K_2CO_3 \ (\text{solid}) \tag{5}$$
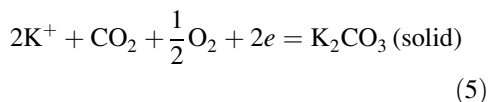
The gas is converted into the immobile ion of the electrolyte. Sensors of this type are called Type II. The EMF of the $CO_2 - O_2$ concentration cell is given by

$$E = \frac{RT}{2F} \ \ln \left\{ \frac{P_{CO_2}^{II} \ (P_{O_2}^{II})^{1/2}}{P_{CO_2}^I \ (P_{O_2}^I)^{1/2}} \right\} \tag{6}$$

$$= \frac{RT}{2F} \ \ln \frac{P_{CO_2}^{II}}{P_{CO_2}^I} \ (for \ P_{O_2}^I = P_{O_2}^{II}) \tag{7}$$

If $P_{O_2}^I = P_{O_2}^{II}$, a simple CO_2 concentration cell results, enabling one to estimate $P_{CO_2}^{II}$ from E for known $P_{CO_2}^I$. The validity of Eq. (7) was confirmed experimentally [2,3].

Obviously the membrane made with an oxyacid salt like K_2CO_3 would not be acceptable in practice. The membrane should be free of pin holes, exhibit adequate levels of ionic conductivity, and mechanically, chemically and thermally stable. A great deal of effort has been exerted to develop better membrane materials, particularly for SO_2 sensors. Various membrane containing metal sulfates such as Ag_2SO_4-K_2SO_4 [4] and Na_2SO_4-Li_2SO_4-$Y_2(SO_4)_3$-SiO_2 [5] have been shown to provide fairly good SO_2 sensing properties when adopted in prototype devices. However, the feasibility of practical sensors using them is yet to be determined.

2.3   Type III Sensors

Another important breakthrough was made by the research group of Saito and Maruyuma [6]. They fabricated an electrochemical cell using NASICON ($Na_3Zi_2Si_2PO_{12}$, Na^+-ionic conductor) to test its response to SO_2. Surprisingly the device did respond to SO_2 in almost the same manner as the device using a Na_2SO_4 membrane. They analyzed the NASICON membrane to find spontaneous formation of Na_2SO_4 on its surface, leading to the following cell structure.

$$SO_2\text{-}O_2\text{-}SO_3, Na_2SO_4, Pt \ ^I | NASICON |^{II}$$
$$Pt, Na_2SO_4, SO_2\text{-}O_2\text{-}SO_3 \tag{8}$$
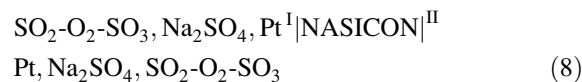
Here SO_3 was produced up to its equilibrium concentration through the oxidation of SO_2 on the electrodes (Pt). This finding is very important, because one can now replace the monolithic membrane of oxyacid salt by a typical solid electrolyte diaphragm attached with the same oxyacid salt, which is far easier to fabricate. The typical solid electrolyte used has nothing to do with the gas to be detected without the aid of the oxyacid salt (auxiliary phase). This type is called Type III. As an extension of this type of sensor, the same group proposed a probe-type CO_2 sensor having an asymmetric cell structure [7].

$$CO_2\text{-air}, Au \ ^I | NASICON \ |^{II} Au, Na_2CO_3, CO_2\text{-air} \tag{9}$$

The interface II combined with Na_2CO_3 is sensitive to CO_2, while interface I is sensitive to O_2 only, so that it is no longer necessary to separate the sample gas (CO_2-air) from the reference gas (O_2 or air). This

probe-type sensor was shown to generate an EMF according to the following equation.

$$E = E_0 + \frac{RT}{2F} \ln P_{CO_2} \qquad (10)$$

where E_0 is constant when T and the sensing materials are fixed. The electrochemical arrangement of this cell will be discussed later (section 6.1).

In the above devices, the main solid electrolyte (NASICON) and the auxiliary phase (Na_2CO_3) have the same mobile ion (Na^+) in common. Later we found that the other types of combinations of solid electrolyte (SE) and auxiliary phase (AP) such as NASICON/Li_2CO_3 and MgO-stabilized zirconia/Li_2CO_3 are also possible. It is more convenient to classify Type III sensors into three subtypes according to the relation between the mobile ions of the SE and the AP as follows.

Table 1 illustrates schematic cell structures for these subtypes together with other types [2,3,7–22]. It is remarked that, to complete an electrochemical cell of IIIb or IIIc, one needs the presence of a mediating layer (ionic bridge) between the SE and the AP. Such ionic bridges are formed spontaneously in many cases. Type III sensors have increased the degree of freedom in sensor design and materials selection dramatically.

3. Fabrication of Type III Sensors

A few Type III sensor devices that we constructed for experimental purposes are shown in Fig. 1. These were unattached with an internal heater and tested in a gas flow apparatus equipped with external heating facilities. For the convenience of device fabrication, gas-separation type devices like (a) (a′) and (b) were mostly used. Since the counter (reference) electrodes of Type III devices are usually insensitive to the gases of interest, a probe type device like (c) is possible.

Structures (a) and (a′) were adopted for the devices using NASICON. A disc of NASICON fabricated in our laboratory, 8 mm in diameter and 0.7 mm thick, was fixed on the end of a quartz tube with an inorganic adhesive. A layer of auxiliary phase (AP) was deposited on the open surface of the disc by a melting and crystallizing method. That is, the designated part of NASICON disc was dipped into a molten bath of AP and quickly taken out in the air to crystallize AP. This method was found to give a thin, porous layer of

AP tightly adhering to the NASICON disc. The sensing electrode (Pt- or Au-mesh) was attached beneath (a) or over (a′) the AP layer. The reference electrode (Pt black) was attached on the opposite side of the disc and exposed to the atmospheric air.

Structure (b) was adopted specifically to utilize a stabilized zirconia tube of commercial origin. The open tube was coated with a layer of AP from a molten AP bath as above. A planar device (c) was prepared on a tip of stabilized zirconia. In this case, the AP layer was attached by applying a paste of pulverized AP and 5 wt% ethyl cellulose dispersed in α-terpineol on the designated part of the tip, followed by calcining at high temperature (800°C). This device could be fixed easily on the alumina substrate attached with an internal heater.
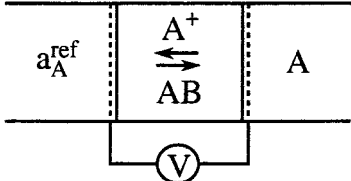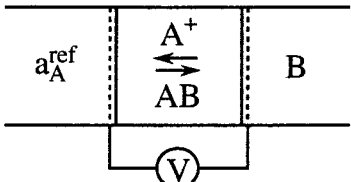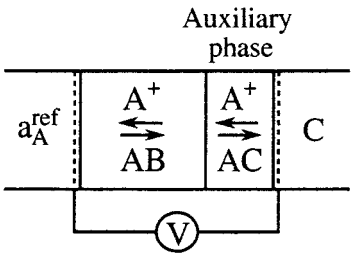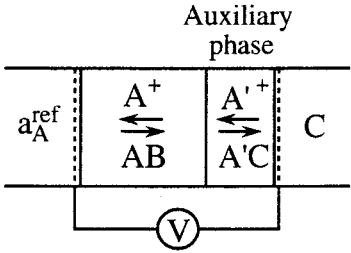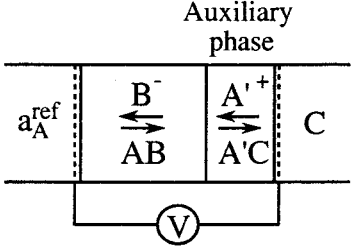
4. NASICON-based Sensors

4.1. NO_x

Concerns about global environmental issues grew sharply in the 1980s, stimulating the development of sensors to detect the hazardous components emitted from combustion facilities. We began our investigation in this field by choosing NO_2 and NO (NO_x) as first targets in 1988. By then, several attempts had been made to develop Type II or III sensors for CO_2 and SO_2, but little attention had been paid to the detection of NO_x despite its importance. NO is produced up to a concentration of a few thousands ppm through the combustion of N-containing fuels (fuel NO_x) as well as the direct reaction between N_2 and O_2 (thermal NO_x). The NO is then oxidized to NO_2 under thermodynamic as well as kinetic constraints. Equilibrium compositions of NO and NO_2 in NO_x are roughly equimolar (1:1) at 500°C under usual conditions, while the ratio of NO or NO_2 increases rather steeply as temperature goes up or down, respectively. The NO_x gases are subjected to NO_x-removal processes before being emitted into the atmosphere. The environmental standard of NO_2 has been legislated to be 40–60 ppb in Japan.

We first tested the possibility of NO_2 sensors of Type IIIa [14]. Electrochemical cells, similar to structure (a) in Fig. 1, were constructed on a disc of Na-β/β″-alumina or NASICON and attached with a layer of $NaNO_3$ as an AP material. The resulting devices were found to respond fairly well to

Table 1. Classification of solid electrolyte gas sensors

Type	Cell structure	Solid electrolyte	Gas
Type I	a_A^{ref} A^+ $\rightleftarrows$ AB A (V)	$ZrO_2(+Y_2O_3)$ $HUO_2PO_4\,4\,H_2O$ $Sb_2O_5\,2\,H_2O$	O_2 H_2[8] H_2[9]
Type II	a_A^{ref} A^+ $\rightleftarrows$ AB B (V)	$Li_2SO_4 - Ag_2SO_4$ Na_2SO_4 $Ba(NO_3)_2 - AgCl$ K_2CO_3 $SrCl_3 - KCl$	SO_X[10] SO_X[11] NO_2[2] CO_2[3] Cl_2[12]
Type IIIa	Auxiliary phase a_A^{ref} A^+ $\rightleftarrows$ AB A^+ $\rightleftarrows$ AC C (V)	Auxiliary phase β-alumina (Na_2SO_4) β-alumina $(NaNO_3)$ NASICON (Na_2CO_3) Li^+-conductor (Li_2CO_3) LaF_3 (LaOF)	SO_X[13] NO_2[14] CO_2[7] CO_2[15] O_2[16]
Type IIIb	Auxiliary phase a_A^{ref} A^+ $\rightleftarrows$ AB A'^+ $\rightleftarrows$ $A'C$ C (V)	Auxiliary phase NASICON (Li_2CO_3) NASICON $(Ba(NO_3)_2)$	CO_2[17] NO_X[18]
Type IIIc	Auxiliary phase a_A^{ref} B^- $\rightleftarrows$ AB A'^+ $\rightleftarrows$ $A'C$ C (V)	Auxiliary phase $ZrO_2\,(+MgO)$ (Li_2SO_4) $ZrO_2(+MgO)$ (Li_2CO_3) $ZrO_2(+MgO)$ $(Ba(NO_3)_2)$ LaF_3 (Li_2CO_3)	SO_X[19] CO_2[20] NO_X[21] CO_2[22]

a_A^{ref} : Activity of A^+ for the reference electrode

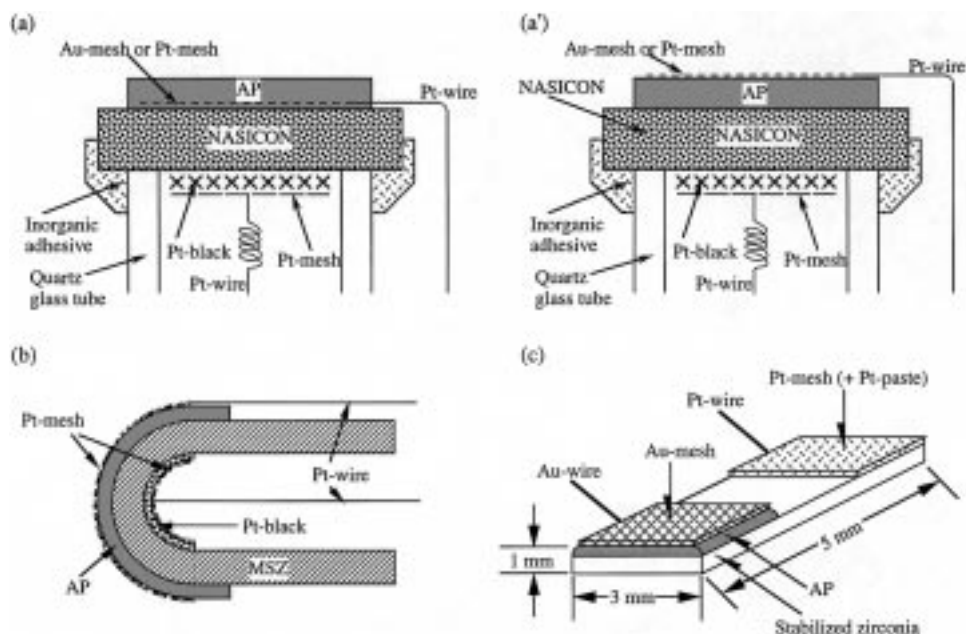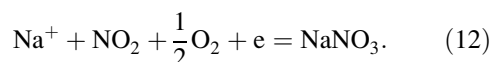AB: Solid electrolyte (A^+ or B^--conductor)

Fig. 1. Structures of Type III sensors. AP: Auxiliary Phase, MSZ: MgO-Stabilized Zirconia.

10–200 ppm NO_2 in air in the temperature range 200–250°C. The EMF response followed the Nernst equation of the form,

$$E = E_0 + \frac{RT}{F} \ln P_{NO_2} \qquad (11)$$

suggesting a sensing electrode reaction of

$$Na^+ + NO_2 + \frac{1}{2}O_2 + e = NaNO_3. \qquad (12)$$

A problem about these devices was that the operating temperature was limited to be up to the melting point of $NaNO_3$ (309°C). This limitation can be serious for applications in combustion-exhaust monitoring. Thus we tried to replace it by $Ba(NO_3)_2$ (melting point 592°C) or a binary nitrate system of $Ba(NO_3)_2 - NaNO_3$ [18]. The device using the binary system was found to be able to operate at 450°C as well as 200°C. Another device using $Ba(NO_3)_2$ could work well at these temperatures provided that the solid electrolyte disc (Na-β/β′-alumina) was ion-exchanged with Ba^{2+} by dipping it in a molten salt of $Ba(NO_3)_2 - BaCl_2$ (62:38 in molar ratio) overnight before use. Unfortunately the introduction of $Ba(NO_3)_2$ was found to induce a serious adverse

affect; the devices showed high cross-sensitivity to CO_2, making the devices unable to work as NO_2 sensors in combustion exhausts. This finding was disappointing with respect to the development of high temperature NO_2 sensors, but at the same time it gave an important hint for designing CO_2 sensors as mentioned later. The possibility of NO_x sensing at high temperature was subsequently pursued with devices working on a different principle (mixed potential) and fairly promising results have been obtained [23]. Type III devices, on the other hand, have been innovated for NO_2 sensing performances at moderate temperature by the discovery of an attractive AP of $NaNO_2$ as mentioned below.

By the way, detection of NO is also very important as a precursor of NO_2. Chemical properties of NO are totally different from those of NO_2 so that it is hardly possible to detect both gases with a single sensor. In fact, the NO_2 sensors fabricated above hardly gave a reasonable response to NO. There are two alternative ways of NO_x detection in practice, i.e., those gases are detected respectively with different sensors, or the concentration of total NO_x is evaluated with an NO_2 or NO sensor after the gases are completely equilibrated or converted into a single component of

NO_2 or NO. We pursued the former way tentatively and tried to develop a Type III NO sensor using NASICON [24]. As for the AP material of the device, $NaNO_2$ was considered. If $NaNO_3$ works for NO_2 sensing, then $NaNO_2$ should work for NO sensing as follows.

$$Na^+ + NO + \frac{1}{2}O_2 + e = NaNO_2 \qquad (13)$$
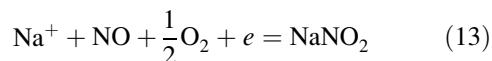
The device using $NaNO_2$ was found in fact to give good sensing properties to NO, as shown in Fig. 2. The subsequent cross-sensitivity test, however, revealed a surprising fact that the device was far better suited to NO_2 sensing. The device gave EMF response to NO_2 in coincidence with the Nernst equation for the one-electron cathodic reaction of NO_2,
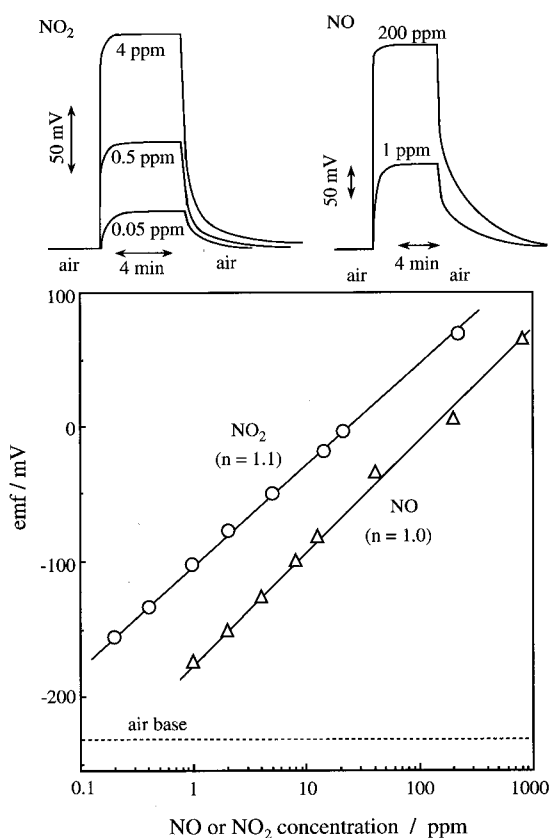
$$Na^+ + NO_2 + e = NaNO_2 \qquad (14)$$

Fig. 2. Dependence of emf of the device attached with $NaNO_2$ auxiliary material on NO or NO_2 concentration. (150°C, structure (a′)).

The EMF response to NO_2 was far larger than that to NO of the same concentration together with very sharp response transients, as also shown in Fig. 2. In addition, the NO_2 sensing performances were far better than those of the previous device using $NaNO_3$, probably in part due to the simplicity of the electrode reaction (14) as compared with (12). These results shows that the $NaNO_2$-attached device, though not applicable for NO sensing under the coexistence of NO_2, can be very attractive as an NO_2 sensing device. Thus we switched back to the NO_2 sensing study again.

The device combined with $NaNO_2$ could satisfactorily detect 0.2–200 ppm NO_2 in air at 150°C in laboratory tests. These performances seemed to be sufficient for applications to combustion exhausts after heat exchange. When tested for various gas mixtures simulating combustion exhausts, the device showed good sensing performances to NO_x (5–100 ppm) provided that the simulation gases were passed through a catalyst bed to burn hydrocarbons off as well as to oxidize NO to NO_2, prior to contacting the device [25].

The lower detection limit (LDL) can be defined as the concentration of NO_2 below which the EMF deviates from the Nernstian relation. For the above particular device, the LDL was about 0.2 ppm at 150°C, which is still far larger than the environmental standard of NO_2 (40–60 ppb). An attempt was made to lower LDL by modifying the $NaNO_2$ with additives. The addition of Li_2CO_3 or Na_2CO_3 turned out to be fairly effective in this respect, although too much additive induced cross-sensitivity to CO_2 [27]. The AP materials of $NaNO_2$-Li_2CO_3 (9:1 in molar ratio), optimized from LDL and CO_2 cross-sensitivity, eventually gave excellent sensing performance down to 5 ppb NO_2 in air without being disturbed by CO_2 of concentration up to 50%, as shown in Fig. 3. Obviously this device has sufficient sensitivity to monitor the environmental NO_2.

Some additional comments regarding the LDL are warranted. All of the above devices exhibit a certain value of EMF to zero concentration of NO_2 in air (air base), as illustrated in Fig. 3. The concentration at which the Nernstian relation intersects the air base gives the critical detection limit of NO_2. Obviously LDL is closely related with the location of the air base, although LDL was a little larger than the critical detection limit. The lowering of LDL with the Li_2CO_3 additive mentioned above resulted mainly from
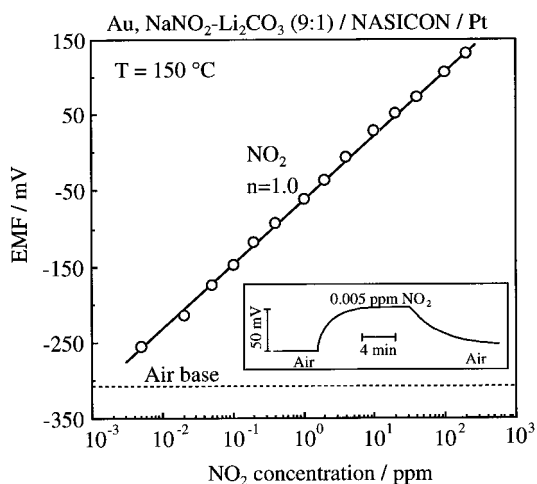
Fig. 3. Dependence of EMF on the concentration of NO_2 (structure (a')).

Fig. 4. Response transients for the sensors using Na_2CO_3 (a and b) and Na_2CO_3-$BaCO_3$ (c and d). (structure (a)) (a) and (c) : Dry CO_2, (b) and (d) : Wet CO_2 (5.3 torr H_2O).

shifting the air base downward relative to the Nernstian relation to NO_2. Beside the AP materials, however, operating temperature and device structure were also important. That is, LDL tended to be lowered as temperature decreased. Further device structure (a') was superior to (a) for obtaining better LDL. These phenomena are rather complex and need further investigation.

4.2. CO_2

As mentioned previously, the device with the $NaNO_3$-$Ba(NO_3)_2$ addition for NO_2 detection was found to suffer from heavy cross-sensitivity to CO_2. This suggests that the AP material was converted into carbonates under the exposure to CO_2. Thus, devices with Na_2CO_3-$BaCO_3$ were fabricated by the melting- and -crystallizing method and tested for CO_2 detection [28]. As it turned out, excellent sensing properties to CO_2 could be obtained at temperatures around 500°C, when the composition of Na_2CO_3-$BaCO_3$ was 1:1.7 in molar ratio or more rich in $BaCO_3$ content. The response transients of a typical device with Na_2CO_3-$BaCO_3$ (1:1.7) are compared with those of a device with Na_2CO_3 only in Fig. 4. Apparently, the former device exhibited far larger EMF response (increment of EMF) to a fixed concentration of CO_2, far sharper response transients, and far greater stability to interference by water vapor than the latter device. The serious interference by water vapor in the latter
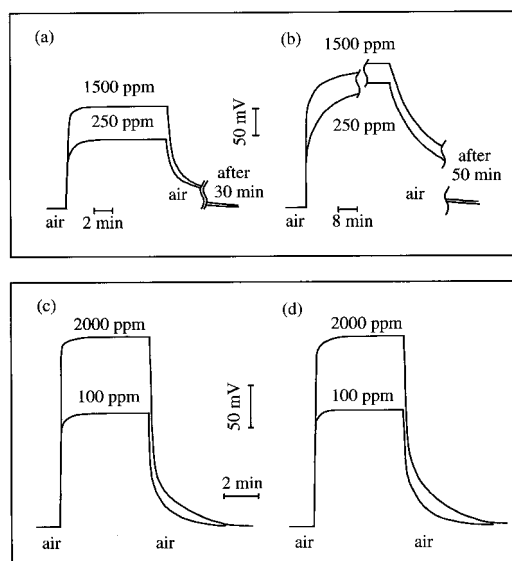
device seemed to show up because Pt sensing electrodes were used at this stage of the investigation. It has been reported that Pt electrodes can be corroded in alkaline atmosphere so that it is better replaced by Au electrodes. Nevertheless the Pt electrode could be used without problem in the former device. This follows from the fact that no crystalline phase of Na_2CO_3 was detected for this device by X-ray diffraction analysis [28].

The EMF of the device to CO_2 obeyed very well the following Nernst equation over a wide range of CO_2 concentration from 10 ppm to 40%, as shown in Fig. 5.
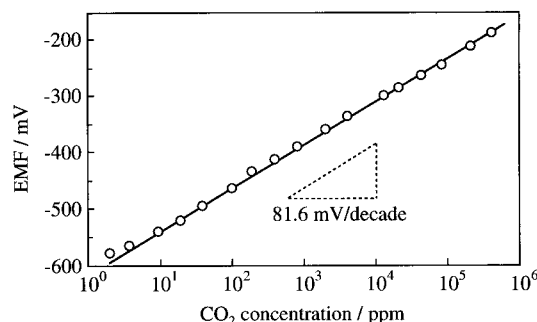

Fig. 5. EMF vs. CO_2 concentration for the device using $BaCO_3$-Na_2CO_3 (1.7:1). (550°C, structure (a)).

$$E = E_0 + \frac{RT}{2F} \ln P_{CO_2} \qquad (15)$$

As judged from these sensing properties, the device seemed to be a very good CO_2 sensor. However, we soon encountered an unexpected problem. The Na_2CO_3-$BaCO_3$ composite was too hygroscopic at room temperature. It deliquesced when the device was kept under humid conditions at room temperature overnight. The deliquescence is obviously induced by Na_2CO_3, and we had to delete it from the device to overcome the problem. Thus the adoptability of Li_2CO_3 was tested. The resulting device, Type IIIb, was found to work fairly well as a CO_2 sensor. In addition, its composites with alkali earth metal carbonates, i.e., Li_2CO_3-$BaCO_3$, Li_2CO_3-$SrCO_3$ and Li_2CO_3-$CaCO_3$, gave better CO_2-sensing performances than the single phase Li_2CO_3. As shown in Fig. 6, for example, the device with Li_2CO_3-$CaCO_3$ (1.8:1 in molar ratio) exhibited excellent sensing performance at 500°C. These devices were hardly disturbed by water vapor, and stable to storage at room temperature under humid condition. These devices now seem to be acceptable for indoor CO_2 monitoring.

Investigations are under way for why the composite auxiliary materials like Na_2CO_3-$BaCO_3$ and Li_2CO_3-$CaCO_3$ give better CO_2 sensing properties than the pure materials like Na_2CO_3 and Li_2CO_3. It has been revealed that the interfaces between NASICON and the carbonate auxiliary materials are not simple, containing corroded or mediating layers more or less in between. It appears that more favorable interface structures are obtained by the use of composite materials.

5.   Stabilized Zirconia-based Sensors

5.1. SO_2

As already mentioned, a device combining NASICON with Na_2SO_4 had been reported as a pioneering work on Type III SO_2 sensor when we began our work. The auxiliary material of this device (Na_2SO_4) was formed spontaneously. This fact arouses apprehension for the long-term stability of the device. One should select a solid electrolyte resistant to corrosive atmospheres at high temperature especially for SO_2 sensors. Stabilized zirconia was considered to be most reliable if adoptable. We selected MgO(15 mol%)-stabilized zirconia (MSZ) because it is more resistant to thermal shock during the sensor fabrication processes than Y_2O_3- or CaO-stabilized zirconia (YSZ or CSZ).

To fabricate a sensing device of structure (c) in Fig. 1, an MSZ tube with a closed end of commercial origin was coated with an auxiliary phase (AP) of metal sulphate by a melting- and -crystallizing method, and then with the sensing electrode (Pt-mesh) and counter electrode (Pt black). When exposed to the flow of SO_2 diluted in air, the device forms the following electrochemical cell (Type IIIc).

$$air, Pt^I \mid MSZ \mid AP \mid {}^{II}Pt, SO_2 - O_2 - SO_3$$
$$(16)$$
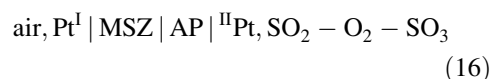
SO_3 is assumed to be produced through the oxidation of SO_2 over the Pt electrode up to its equilibrium composition.

$$SO_2 + \frac{1}{2}O_2 = SO_3, K = \frac{P_{SO_3}}{P_{SO_2} \cdot P_{O_2}^{1/2}} \qquad (17)$$
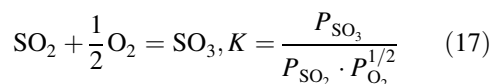
Here K is the equilibrium constant.

Figure 7 illustrates SO_2 sensing properties of the device with Li_2SO_4 at 650 and 800°C. The response to switching-on SO_2 was rapid but the recovery upon switching-off SO_2 was rather sluggish at both temperatures. The EMF to SO_2 under constant oxygen concentration obeyed the following equation.

$$E = E_0 + \frac{RT}{2F} \ln P_{SO_{2,in}} \qquad (18)$$

Here $P_{SO_{2,in}}$ stands for the partial pressure of the inlet SO_2 which is equal to the sum of P_{SO_2} and P_{SO_3}.

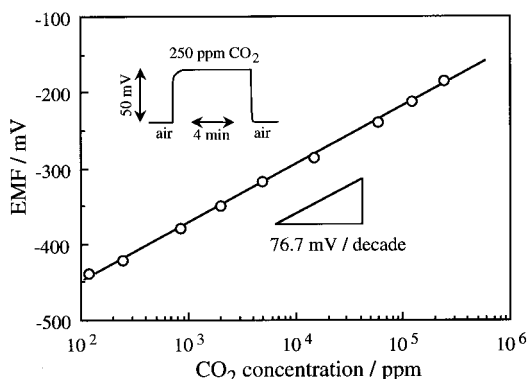Fig. 6. Response transient and EMF to CO_2 for the NASICON based device with Li_2CO_3-$CaCO_3$. (500°C, structure (a)).

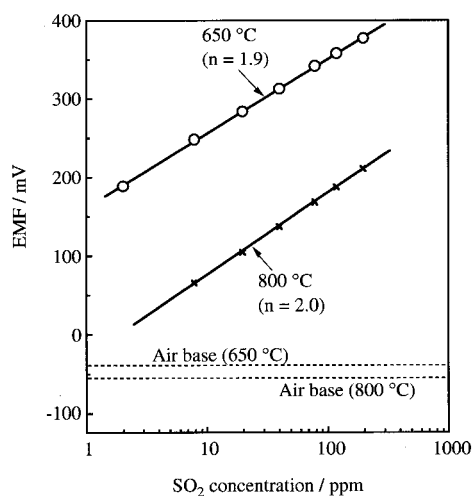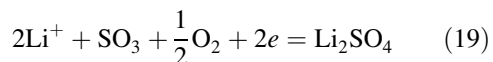*Fig. 7.* Correlations between EMF and inlet SO_2 concentration for the MSZ-based device fitted with Li_2SO_4 at 650 and 800°C. (structure (b)).

Fig. 8. Response transients and stability of EMF vs inlet SO_2 concentration correlation in three weeks for the MSZ-based device attached with Li_2SO_4-$CaSO_4$-SiO_2 (4:4:2) at 650°C. (structure (b)).

This equation can be explained based on the sensing electrode reaction

$$2Li^+ + SO_3 + \frac{1}{2}O_2 + 2e = Li_2SO_4 \qquad (19)$$

and the assumption of equilibrium for the reaction [17]. The EMF to a fixed concentration of SO_2 shifted down rather steeply on increasing temperature, while the air base remained rather fixed. This means that the lower detection limit (LDL) depends on temperature. As suggested from Fig. 7, LDL will be smaller than 0.1 ppm SO_2 at 650°C, while it will be around 1 ppm at 800°C. Similar SO_2 sensing properties were also obtained with the device with Na_2SO_4. It will be possible to apply this type of device for monitoring environmental SO_2 (standard 40 ppb in Japan) if lower operating temperatures are available.

Attempts were made to optimize the auxiliary material from the viewpoint of response kinetics, especially the rate of recovery [29]. The rate of recovery was improved considerably when Li_2SO_4 was replaced by a binary system of Li_2SO_4-$CaSO_4$ (6:4 in molar ratio). The fastest recovery was provided with a ternary system of Li_2SO_4-$CaSO_4$-SiO_2 (4:4:2 in molar ratio), as shown in Fig. 8. The time for 90% recovery was 2–4 min to be compared to 34–40 min for the device with Li_2SO_4. This device exhibited good stability in operation for the medium test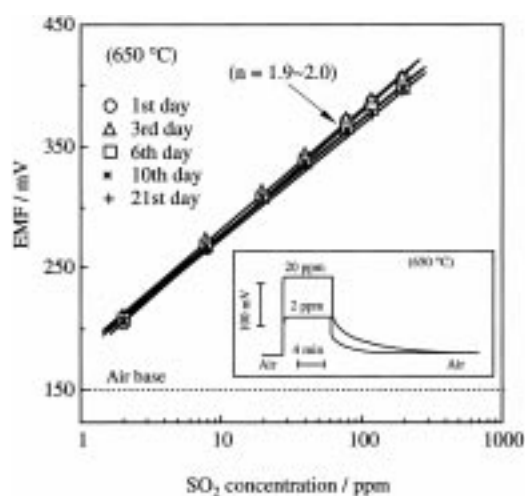ed, as also shown in Fig. 8. As judged from SEM observations of the auxiliary materials as well as the cross-sections of the devices, the addition of $CaSO_4$ and SiO_2 seems to improve the adhesion of the AP layer to MSZ and to eliminate cracks and macropores from the AP layer, respectively, as illustrated schematically in Fig. 9.

YSZ or CSZ tubes in place of the MSZ tube were later tried [30]. Unexpectedly the YSZ- or CSZ- based devices with Li_2SO_4 failed to give a stable response to
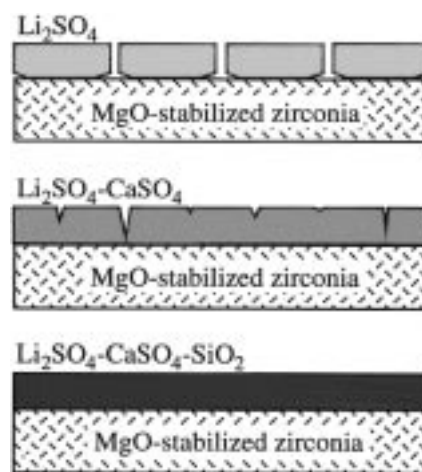

Fig. 9. Schematic drawings of the morphology of auxiliary phases coated on MSZ.

SO_2. It was found, however, that the devices could work well when the auxiliary material was replaced by Li_2SO_4-MgO (8:2 in molar ratio), indicating the importance of MgO. Further, it turned out that the MSZ tubes used in these studies happened to contain a certain amount of free MgO. When a well-prepared MSZ tube was used, the MgO-mixed auxiliary material (Li_2SO_4-MgO) was again necessary to obtain a reasonable response to SO_2. Thus, MgO is required to form an ionic bridge (probably MgO-Li_2ZrO_3 solid solution) which mediates between stabilized zirconia (O^{2-} conductor) and the auxiliary material (Li^+ conductor).

5.2. CO_2

It was found that a CO_2 sensor of the same type (IIIc) could be obtained by combining an MSZ tube with an auxiliary material of Li_2CO_3 [20]. The correlation between EMF and CO_2 concentration at temperatures in the range 550–650°C as well as response transients at 550°C are shown in Fig. 10. The response and recovery were sharp. The EMF obeyed the same Nernst Eq. (18) as already observed with the NASICON-based device. Unlike the previous case, however, the EMF was found to be dependent on the concentration of coexistent oxygen over the temperature range examined. This dependence on oxygen concentration could be completely removed when a probe-type planar device of structure (c) was used.
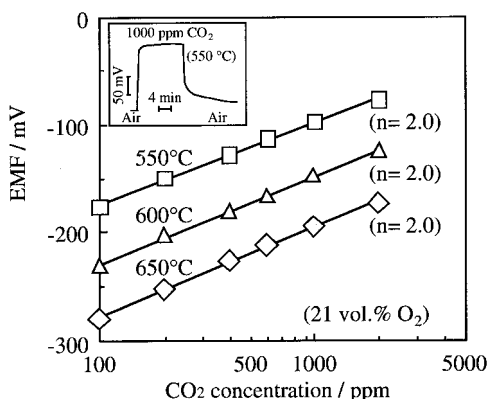
6. Electrochemistry of Hetero-junctions

6.1. Electrochemical Chain

Every sensor of Type III has a hetero-junction between the base solid electrolyte (SE) and the auxiliary phase (AP). An electrochemical chain must be established through the junction. For a Type IIIa device, this is straight forward. Let us consider the NASICON-based CO_2 sensor shown in Fig. 11. This device can be considered as coupling an O_2-sensitive half cell (left) with a CO_2-sensitive one (right). Since SE and AP have the same mobile ion (Na^+) in common, the electrochemical chain is easily achieved with Na^+. The electrochemical potential of Na^+ is defined as

$$\bar{\mu}_{Na^+} = \mu_{Na^+} + F\phi \qquad (20)$$

where μ_{Na^+} is chemical potential of Na^+ and ϕ is electric potential. μ_{Na^+} is different for SE and AP and, in the vicinity of the sensing and counter electrodes, it changes with a change in O_2 or CO_2 concentration. The equilibrium condition requires that $\overline{\mu_{Na^+}}$ be equal through out the device. To achieve this, ϕ also changes to compensate the change of μ_{Na^+}, leading to the generation of EMF for the device. For the particular device using Na_2CO_3, the electrochemical reactions on the sensing and counter electrodes have been proposed by Saito and Maruyama [7] as follows.
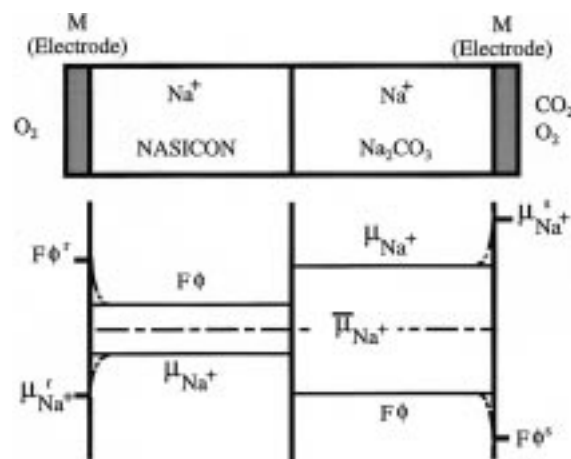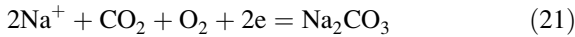

Fig. 10. Correlations between EMF and CO_2 concentration for the MSZ-based device attached with Li_2CO_3 at three temperatures.

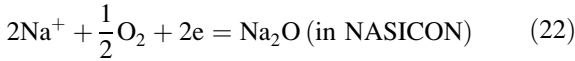

Fig. 11. Electrochemical chain diagram of a CO_2 sensor using NASICON / Na_2CO_3 combination (Type IIIa, structure (a')).

Sensing electrode :

$$2Na^+ + CO_2 + O_2 + 2e = Na_2CO_3 \qquad (21)$$

Reference electrode :

$$2Na^+ + \frac{1}{2}O_2 + 2e = Na_2O \text{ (in NASICON)} \qquad (22)$$

Overall reaction :

$$Na_2O \text{ (in NASICON)} + CO_2 = Na_2CO_3 \qquad (23)$$

The Gibbs' free energy change (ΔG) of the overall reaction is positive at the temperature of interest (around 500°C), indicating that the reaction actually tends to proceed in the reverse direction. The EMF is given by $-\Delta G/2\mathbf{F}$, which is negative for the cell arrangement above. Recently, Holzinger et al. reported Na-β'-alumina-based CO_2 sensors (Type IIIa) attached with a CO_2-sensitive auxiliary phase of Na_2CO_3 (sensing electrode) and an O_2-sensitive auxiliary system of $Na_2O - TiO_2$ (reference electrode). They showed a CO_2 sensing mechanism which is similar to the above one [31].

For Type IIIb and IIIc devices, an electrochemical chain can not be attained without the presence of a mediating phase (ionic bridge) between SE and AP. Let us consider the CO_2 sensor which couples MSZ (SE) and Li_2CO_3 (AP) as shown in Fig. 12. The left half cell sensitive to O_2 and the right one sensitive to CO_2 are governed by and $\overline{\mu_{O^{2-}}}$, and $\overline{\mu_{Li^+}}$, respectively. The two function can be correlated to each other only when there is an interfacial compound which contains both ions. As such a compound, Li_2ZrO_3 is assumed
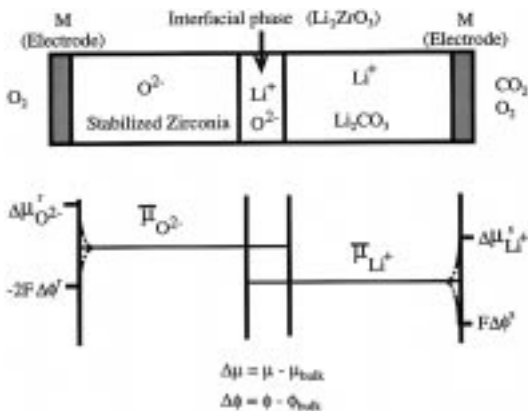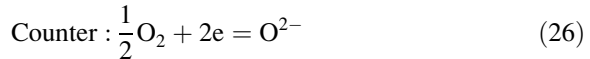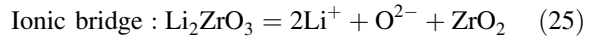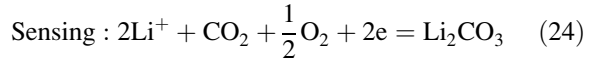
here. Then we can write down all the cell reactions as follows.

$$\text{Sensing}: 2Li^+ + CO_2 + \frac{1}{2}O_2 + 2e = Li_2CO_3 \quad (24)$$

$$\text{Ionic bridge}: Li_2ZrO_3 = 2Li^+ + O^{2-} + ZrO_2 \quad (25)$$

$$\text{Counter}: \frac{1}{2}O_2 + 2e = O^{2-} \qquad (26)$$

Overall :

$$CO_2 + Li_2ZrO_3 = Li_2CO_3 + ZrO_2, \Delta G \qquad (27)$$

The device EMF, $-\Delta G/2\mathbf{F}$, is thus dependent on the kind of ionic bridge involved. For the above device, the observed EMF was very close to what is expected from the ionic bridge of Li_2ZrO_3, as shown in Fig. 13 [32]. It is possible to complete the cell reaction by assuming an ionic bridge of Li_2O, but this assumption leads to a great discrepancy between the theory and the practice, as also shown.

For the other sensors of Type IIIb or IIIc, ionic bridges appear to be more complex. For the SO_2 sensors using stabilized zirconia and metal sulphates, the ionic bridge seems to be provided by MgO-containing Li_2ZrO_3, not simply by Li_2ZrO_3. For the CO_2 sensors using NASICON and Li_2CO_3-based auxiliary materials, formation of a solid solution containing Na^+ and Li^+ is highly probable.

6.2. Dual Chains

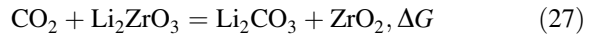Type III devices of structure (a) have the sensing electrode sandwiched between SE and AP. Let us

Fig. 12. Electrochemical chain diagram of a CO_2 sensor using MSZ / Li_2CO_3 combination (Type IIIc, structure (b) or (c)).
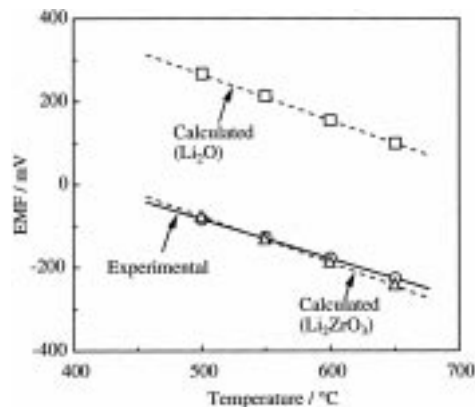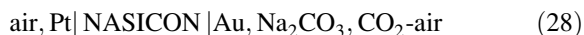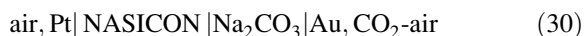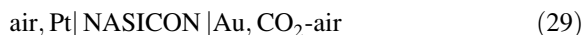

Fig. 13. Correlations between EMF to 400 ppm CO_2 and temperature for the MSZ-based device with Li_2CO_3. (structure (c)).

consider the CO_2 sensor combining NASICON and Na_2CO_3 of the form

$$air, Pt| \text{ NASICON } |Au, Na_2CO_3, CO_2\text{-air} \qquad (28)$$

It is easily understood that the Au sensing electrode is involved in two kinds of three-phase contacts, i.e., one among Au, SE and gas phase and the other among Au, AP and gas phase. We can therefore deconvolute the device into two elementary cells.

$$air, Pt| \text{ NASICON } |Au, CO_2\text{-air} \qquad (29)$$

$$air, Pt| \text{ NASICON } |Na_2CO_3|Au, CO_2\text{-air} \qquad (30)$$

The first one is a cell sensitive to O_2, while the second one is the same CO_2-sensing cell we just discussed. These cells are connected in parallel, sharing the same electrodes. It has been shown that the EMF of the device is determined by the competition between the two cells [33]. In the higher temperature region the CO_2-sensing cell is more influential than the O_2-sensitive one, while the reverse is true in the lower temperature region. This results in the appearance of lower limiting temperature for CO_2 detection, which is about 400°C for the Na_2CO_3-attached device, as shown in Fig. 14. It has been shown that the lower limiting temperature can be lowered to 350°C or below when a binary system like Li_2CO_3-$CaCO_3$ is used for AP.
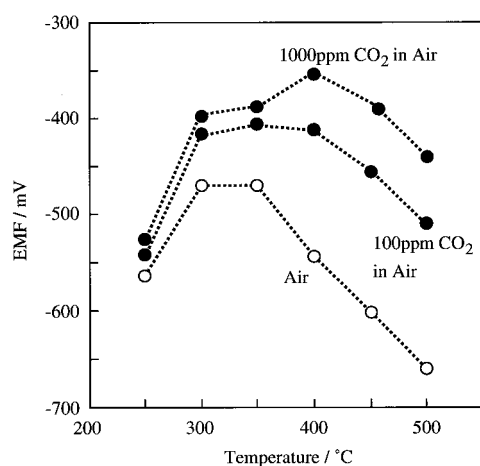

Fig. 14. EMF values of the NASICON-based device with Na_2CO_3 to 0, 100, or 1000 ppm CO_2 in air as correlated with temperature. (structure (a)).

7.   Prospect and Problems

Table 2 summarizes several sensors of Type III for CO_2, NO, NO_2 and SO_2. These sensors have shown attractive performances in short term laboratory tests, though most of them should be subjected to field and long term stability tests. Among these, the CO_2 sensors may be applicable for auto-ventilation of indoor air as well as for CO_2 control in green houses. As CO_2 is deeply associated with bioactivities of animals, plants and bacteria, the sensors may also be applicable to measurement or control of various bioactivities. The NO_2 sensors have restricted applicability to emission control for combustion exhausts because of the upper limit of operating temperature. Instead there is ample possibility of monitoring NO_2 and possibly total NO_x in environmental atmospheres by using these sensors. The SO_2 sensors have intrinsic capability of monitoring SO_2 in combustion exhausts, and may also be applicable to environmental SO_2 monitoring.

It has to be mentioned that these sensors still have many problems, from basic to technical, to be solved. Some are as follows.

1. For NASICON-based sensors for CO_2, NO and NO_2, the EMF is independent of P_{O_2}, inconsistent with the sensing electrode reactions assumed (Eq. (12), (13) and (21)). The gas sensing reactions, especially the dependence on O_2, should be elucidated.
2. For these devices, air base is a major factor to determine the lower detection limit for the gas of interest. The nature of the air base should be clarified.
3. Hetero-junctions and ionic bridges between SE and AP have great importance for the performance and stability of the devices. Their structure and properties should be clarified.
4. Various kinds of AP have been used empirically so far. Principles of AP design should be established.
5. The operating temperatures of the devices are not always well suited to their applicational purposes. For example, lower temperature will be more favorable for usual purposes, while sufficiently high temperature will be needed for combustion exhausts control. It is desired to make the operating temperature more flexible.

If these problems are solved, we can move a great step forward towards establishing excellent sensors for oxidic gases.

Table 2. Gas sensing performance of Type III sensors

Gas	Solid electrolyte	Auxiliary material	Operating temp./°C	Time for 90% response/sec	Dynamic range of detection (tested)
CO_2	NASICON	Na_2CO_3-$BaCO_3$	550	<8	4 ppm $\sim$ 40%
		Li_2CO_3-$CaCO_3$	500	<8	''
		Li_2CO_3-$BaCO_3$	550	<8	''
			270	60	''
NO_2	NASICON	$NaNO_3$	150	60	1 $\sim$ 200 ppm
		$NaNO_3$-$Ba(NO_3)_2$	200 $\sim$ 450	60	1 $\sim$ 200 ppm
		$NaNO_2$	150 $\sim$ 225	<8	0.1 $\sim$ 200 ppm
		$NaNO_2$-Li_2CO_3	150	<8	0.005 $\sim$ 200 ppm
NO	NASICON	$NaNO_2$	150 $\sim$ 225	<8	1 $\sim$ 800 ppm
SO_2	MgO-stabilized zirconia	Li_2SO_4-$CaSO_4$	700	<10	2 $\sim$ 200 ppm
		Li_2SO_4-$CaSO_4$ $-$ SiO_2	650	<10	2 $\sim$ 200 ppm

References

1. W. Weppner, in *Proc. 2nd Int. Meeting on Chemical Sensors*, 59–68 (1986).
2. M. Gauthier and A. Chamberland, *J. Electrochem. Soc.*, **124**, 1579–1583 (1977).
3. R. Côtè, C.W. Bale, and M. Gauthier, *J. Electrochem. Soc.*, **131**, 63–67 (1984).
4. W.L. Worrell, in *Proc. 1st Int. Meeting on Chemical Sensors*, 332–337 (1983).
5. N. Imanaka, Y. Yamaguchi, G. Adachi, and J. Shiokawa, *J. Electrochem. Soc.*, **134**, 725–728 (1987).
6. Y. Saito, T. Maruyama, Y. Matsumoto, K. Kobayashi, and Y. Yano, *Solid State Ionics*, **14**, 273–281 (1984).
7. T. Maruyama, S. Sasaki, and Y. Saito, *Solid State Ionics*, **23**, 107–112 (1987).
8. J.S. Lundsgaard, J. Malling, and M.L.S. Birchall, *Solid State Ionics*, **7**, 53–56 (1982).
9. N. Miura and N. Yamazoe, *Solid State Ionics*, **23–56**, 975–982 (1992).
10. W.L. Worrell, *Chemical Sensor Technology*, **1**, 97–108 (1988).
11. K.T. Jacob and D.B. Rao, *J. Electrochem. Soc.*, **126**, 1842–1847 (1979).
12. A. Pelloux, P. Fabry, and P. Durante, *Sensors and Actuators*, **7**, 245–252 (1985).
13. R. Akila and K.T. Jacob, *Sensors and Actuators*, **16**, 311–323 (1989).
14. Y. Shimizu, Y. Okamoto, S. Yao, N. Miura, and N. Yamazoe, *Denki Kagaku*, **59**, 465–472 (1991).
15. N. Imanaka, T. Kawasato, and G. Adachi, *Chem. Lett.*, **1990**, 497–500 (1990).
16. N. Miura, J. Hisamoto, N. Yamazoe, S. Kuwata, and J. Saladenne, *Sensors and Actuators*, **16**, 301–310 (1989).
17. S. Yao, S. Hosohara, Y. Shimizu, N. Miura, H. Futata, and N. Yamazoe, *Chem. Lett.*, **1991**, 2069–2072 (1991).
18. N. Miura, S. Yao, Y. Shimizu, and N. Yamazoe, *Sensors and Actuators*, **B 13–14**, 387–390 (1993).
19. Y. Yan, Y. Shimizu, N. Miura, and N. Yamazoe, *Chem. Lett.*, **1992**, 635–638 (1992).
20. N. Miura, Y. Yan, M. Sato, S. Yao, Y. Shimizu, and N. Yamazoe, *Chem. Lett.*, **1994**, 393–396 (1994).
21. H. Kurosawa, Y. Yan, N. Miura, and N. Yamazoe, *Chem. Lett.*, **1994**, 1733–1736 (1994).
22. N. Miura, S. Yao, M. Sato, Y. Shimizu, S. Kuwata, and N. Yamazoe, *Chem. Lett.*, **1993**, 1973–1976 (1993).
23. N. Miura, H. Kurosawa, M. Hasei, G. Lu, and N. Yamazoe, *Solid State Ionics*, **86–88**, 1069–1073 (1996).
24. S. Yao, Y. Shimizu, N. Miura, and N. Yamazoe, *Chem. Lett.*, **1992**, 587–590 (1992).
25. T. Nakahira, H. Enomoto, T. Setoguchi, H. Taguchi, S. Ishihara, N. Miura, and N. Yamazoe, *Chemical Sensors*, **10** Supplement A, 69–72 (1993).
26. N. Miura, S. Yao, Y. Shimizu, and N. Yamazoe, *Solid State Ionics*, **70/71**, 572–577 (1994).
27. S. Yao, Y. Shimizu, N. Miura, and N. Yamazoe, *Chem. Lett.*, **1990**, 2033–2036 (1990).
28. N. Miura, S. Yao, Y. Shimizu, and N. Yamazoe, *J. Electrochem. Soc.*, **139**, 1384–1388 (1992).
29. Y. Yan, Y. Shimizu, N. Miura, and N. Yamazoe, *Sensors and Actuators*, **B 20**, 81–87 (1994).
30. Y. Yan, N. Miura, and N. Yamazoe, *J. Electrochem. Soc.*, **143**, 609–613 (1996).
31. M. Holzinger, J. Maier, and W. Sitte, *Solid State Ionics*, **86–88**, 1055–1062 (1996).
32. N. Yamazoe and N. Miura, *Solid State Ionics*, **86–88**, 987–993 (1996).
33. N. Yamazoe, S. Hosohara, T. Fukuda, K. Isono, and N. Miura, *Sensors and Actuators*, **B 34**, 361–366 (1996).